

1 Propagation of partially coherent fields radiated by sources 2 with univariable cross-spectral density

3 Massimo Santarsiero¹, Rosario Martínez-Herrero², Juan Carlos González de Sande³, Gemma
4 Piquero^{2,*}, Olga Korotkova⁴, and Franco Gori¹

5 ¹DIEM, Università Roma Tre, via V. Volterra 62, Rome 00146, Italy.

6 ²Departamento de Óptica, Fac. CC. Físicas, U.C.M., Ciudad Universitaria s/n, 28040 Madrid, Spain.

7 ³Universidad Politécnica de Madrid, ETSIS de Telecomunicación, Campus Sur, 28031 Madrid, Spain.

8 ⁴Department of Physics, University of Miami, 1320 Campo Sano Drive, Coral Gables, FL, 33146.

9 **Abstract.** A new class of partially coherent light sources, the sources with
10 uni-variable cross-spectral density, has been recently introduced. Their cross-
11 spectral density is obtained starting from any function of a single complex ar-
12 gument having non-negative Taylor coefficients. This allows the conception of
13 a virtually infinite number of physically realizable partially coherent sources.
14 Here, the main characteristics of sources of this class are investigated through
15 examples, with particular reference to the irradiance and coherence properties
16 across the source plane and upon propagation, both in the near and in the far
17 field. Furthermore, since the coherent modes of such sources present opti-
18 cal vortices, parameters quantifying the vortex structure of the field across the
19 source plane are also evaluated for the presented cases.

20 **Keywords:** Coherence, Coherent modes, Propagation, Optical vortices, Orbital angular moment,
21 Structured coherence

22 1 Introduction

23 Structured light has attracted strong interest in recent years, largely driven by its wide range of applica-
24 tions and by rapid progress in generating and detecting tailored optical fields [1, 2]. Within this area,
25 partially coherent sources are increasingly regarded not as a limitation but as a useful design degree of
26 freedom, since the engineering of spatial coherence can mitigate drawbacks of highly coherent beams.
27 Recent reviews emphasize that partially coherent beams with structured coherence have been explored
28 for concrete applications including: optical imaging [3, 4], free-space optical communications with im-
29 proved robustness to atmospheric turbulence [5–8], coherence-based optical encryption and robust sig-
30 nal/information transmission through complex or scattering media [8, 9], optical manipulation [10, 11],
31 and remote sensing [12]. These are some of the reasons why there is great interest in devising, realizing,
32 and characterizing new light sources, both coherent and partially coherent, that allow the characteristics
33 of the light radiated by these sources to be modified in a controlled way [13–38].

34 Interesting and promising results are derived from the presence of phase vortices, which confers
35 unique capabilities to the beam radiated from the source [5, 6, 12, 39–54]. For example, they find
36 application in optical manipulation, because they can exert torque on microscopic particles, enabling
37 advanced optical tweezers and micromanipulation [10, 46]; in imaging and metrology, where they offer
38 new possibilities for super-resolution or phase-sensitive detection [12, 44]; in optical communication,

*e-mail: piquero@ucm.es

39 since they provide an extra degree of freedom, the orbital angular momentum (OAM), for multiplexing
40 and increasing data capacity [5, 6]. Vortex beams are typically generated using elements such as spiral
41 phase plates, computer-generated holograms, q plates, or metasurfaces that encode the desired OAM
42 mode [47, 50, 51, 53].

43 Recently, a new type of partially coherent light source, namely, sources with uni-variable cross-
44 spectral density (CSD), has been proposed [38]. The peculiarity of sources of this class is that their
45 CSD [55] can be directly derived from a function of a single complex variable [38]. The only require-
46 ment this function has to fulfill in order for it to be associated to a well defined CSD is that its Taylor
47 expansion must involve only non-negative coefficients. Several analytical forms, in some cases very
48 simple, of bona-fide CSD can be devised in this way. Sources with uni-variable CSD are defined within
49 a finite circular region, related to the convergence domain of the above Taylor series, and can be ex-
50 pressed as the superposition of coherent modes [55] carrying optical vortices. The analytical form of
51 the vortex modes is quite simple, both across the source plane and in the far zone, enabling the study
52 of the coherence features of the source, as well as those of the field radiated under Fraunhofer condi-
53 tions [38]. One of the important features of univariable CSDs is their capability to customize at will the
54 contributions from various coherent modes, serving, at the same rate, as the OAM modes. This renders
55 them ideal for high-capacity information-transfer applications employing structured light.

56 The main aim of the present paper is, on one hand, to extend to the Fresnel regime the study of
57 the propagation of beams radiated from sources with uni-variable CSD; on the other hand, to study the
58 effects of truncating the number of the modes involved in the expansion. Examples will be presented,
59 concerning the so-called sZegő source, introduced in [38], which is obtained with an infinite number
60 of Taylor terms, all with the same coefficient. Taking only a finite number of terms gives rise to the
61 truncated sZegő source, introduced here, which represents a more realistic model for a partially coherent
62 source, suitable to be physically realized. Finally, hints for devising other types of uni-variable CSDs
63 are given for some cases in which the CSD takes a simple closed form.

64 2 Preliminaries

65 2.1 Uni-variable CSDs

66 A uni-variable CSD [38] is defined from any function g of a single complex variable ζ such that

$$g(\zeta) = \sum_{n=0}^{\infty} c_n \zeta^n, \quad (1)$$

67 where

$$c_n \geq 0 \quad (\forall n), \quad (2)$$

68 and ζ belongs to the convergence domain of the series. By suitably scaling the argument of g it is always
69 possible to set such a domain as

$$|\zeta| < 1. \quad (3)$$

70 The CSD associated with g is obtained by letting

$$\zeta = \frac{r_1 r_2}{r_0^2} e^{i(\varphi_1 - \varphi_2)}, \quad (4)$$

71 where (r_1, φ_1) and (r_2, φ_2) are the polar coordinates of two points across the source plane (\mathbf{r}_1 and \mathbf{r}_2)
72 and r_0 is the radius of the circular region where the source is defined. It should be noted that although
73 the CSD depends on two points, for this class of sources the dependence enters only through the single
74 complex parameter ζ , following the terminology introduced previously in Ref [38]. Therefore, using
75 Eqs. (1) and (4) we define, across the plane $z = 0$,

$$W(\mathbf{r}_1, \mathbf{r}_2, 0) = g\left(\frac{r_1 r_2}{r_0^2} e^{i(\varphi_1 - \varphi_2)}\right) = \sum_{n=0}^{\infty} c_n \left(\frac{r_1 r_2}{r_0^2}\right)^n e^{in(\varphi_1 - \varphi_2)}, \quad (|r| < r_0). \quad (5)$$

76 The sum in Eq. (5) can be read as the Mercer expansion of W_0 , that is, [55]

$$W(\mathbf{r}_1, \mathbf{r}_2, 0) = \sum_{n=0}^{\infty} \lambda_n \Phi_n(\mathbf{r}_1, 0) \Phi_n^*(\mathbf{r}_2, 0), \quad (6)$$

77 with coherent modes (taken into account their normalization) given by

$$\Phi_n(\mathbf{r}, 0) = \sqrt{\frac{n+1}{\pi r_0^2}} \left(\frac{r}{r_0}\right)^n \text{circ}\left(\frac{r}{r_0}\right) e^{in\varphi}, \quad (n = 0, 1, \dots), \quad (7)$$

78 and eigenvalues

$$\lambda_n = c_n \frac{\pi r_0^2}{n+1}, \quad (n = 0, 1, \dots), \quad (8)$$

79 where $\text{circ}(r)$ is the characteristic function of a unit disk centered at the origin of the axes. The second
80 argument of the modes Φ_n refers to the z -coordinate of the transverse plane where they are evaluated (in
81 this case, across the source, that is, $z = 0$). The condition in Eq. (2), together with Eq. (8), guaranties
82 that $\lambda_n > 0$ ($\forall n$), so that the CSD turns out to be well defined [13, 14].

83 The modes in Eq. (7) are recognized at once as optical vortices [49] with charge n . They have the
84 same structure as Laguerre–Gaussian beams [56] in which the Laguerre polynomial has order zero and
85 where the Gaussian function has been replaced by a circ.

86 The number of genuine CSDs that can be obtained following the present approach is practically
87 unlimited, the only constraint that the function g has to fulfill being the fact that the coefficients of its
88 Taylor expansion are all non-negative. Examples will be given in the following, where simple forms of
89 CSDs will be presented, together with the mean features of the beams they radiate.

90 2.2 Characterization of uni-variable CSDs in OAM space

91 Uni-variable CSD represents one of a few known model optical fields that carry OAM in multiple
92 modes, either finite or infinite. For the characterization of radial-only correlations among the OAM
93 modes in such fields, the coherence–orbital angular momentum (COAM) matrix $\vec{W}(\rho_1, \rho_2, z)$ and its
94 derivatives can be used [57]. Each element of the COAM matrix is a scalar radial field correlation at a
95 pair of OAM indices, given by expression:

$$W_{\ell m}(r_1, r_2, z) = \frac{1}{4\pi^2} \int_0^{2\pi} \int_0^{2\pi} W(\mathbf{r}_1, \mathbf{r}_2, z) e^{-i(\ell\varphi_1 - m\varphi_2)} d\varphi_1 d\varphi_2, \quad -\infty < \ell, m < \infty. \quad (9)$$

96 The COAM matrix is the counterpart of the CSD matrix defined in polarization space to the OAM
97 space and carries similar properties (quasi-Hermiticity, non-negative definiteness, etc.). However, it
98 can have any size, say $L \times L$, where L is the largest by magnitude OAM index involved. Also, for
99 theoretical models, infinitely dimensional matrices are possible with certain convergence constraints.
100 The uni-variable beam model is of this type.

101 Two derivatives of the COAM matrix are important and will be considered here. First, the OAM
102 degree of coherence is the analog of the EM degree of coherence in the OAM space [58]:

$$o(r_1, r_2, z) = \frac{\sqrt{\text{Tr}[\vec{W}^\dagger(r_1, r_2, z) \vec{W}(r_1, r_2, z)]}}{\prod_{j=1,2} \sqrt{\text{Tr} \vec{W}(r_j, r_j, z)}}. \quad (10)$$

103 It provides the cumulative information about the normalized correlations at a pair of radii for all pairs
104 of the OAM modes, regardless from the OAM phase information contained in each mode.

105 Second, it was found that a harmonic beam carrying OAM in L modes traces an orbitalization ellipse
106 in LD OAM space (polar Fourier space) at a fixed radius [59], analogously to the two/three component
107 electric field tracing a polarization ellipse in real 2D/3D space. To extend this geometric description

108 to partially coherent beams, the COAM matrix can be considered at a single radius $r_1 = r_2 = r$, and
109 regarded as the $L \times L$ orbitalization matrix: [60]

$$\overleftrightarrow{O}(r, z) = \overleftrightarrow{W}(r, r, z), \quad (11)$$

110 the term stemming from its formal similarly to a polarization matrix. In LD the orbitalization matrix
111 is shown to decompose into three parts: completely orbitalized, unorbitalized and partially orbitalized
112 in which mixing occurs for mode couples, triples, \dots , up to $L - 1$. The completely orbitalized matrix
113 is shown to factorize, representing a beam indistinguishable from harmonic, and, hence, described by
114 an orbitalization ellipse. The contribution of the intensity of the completely orbitalized portion of the
115 beam in the total beam, at a fixed radius, was introduced as the degree of orbitalization [60]

$$O(r, z) = \frac{\sigma_0(r, z) - \sigma_1(r, z)}{\sum_{n=0}^{\infty} \sigma_n(r, z)}, \quad (12)$$

116 where $\sigma_0(r, z) \geq \sigma_1(r, z) \geq \dots \geq \sigma_L(r, z) \geq \dots$ is the ordered sequence of the eigenvalues of \overleftrightarrow{O} , all being
117 real and nonnegative due to its Hermiticity and non-negative-definiteness. This quantity is analogous
118 in nature to the degree of polarization and reduces to it in form for $L = 2$ and 3. In this work we will
119 thoroughly examine its behavior for uni-variable beams.

120 We note that for a univariable CSD the COAM matrix is diagonal and hence the calculations of
121 both derivatives are relatively simple. For example, the OAM DOC becomes

$$o(r_1, r_2, 0) = \frac{\sqrt{\sum_{n=0}^{\infty} c_n^2 (r_1 r_2 / r_0^2)^{2n}}}{\prod_{j=1,2} \sqrt{\sum_{n=0}^{\infty} c_n (r_j / r_0)^n}}. \quad (13)$$

122 As we show below, for uni-variable beams σ_0 and σ_1 may depend on different c_n at different radii
123 and, hence, it appears impossible to write down an explicit single formula for the degree of orbital-
124 ization. Instead, a piecewise-continuous function will be used, with its interval endpoints determined
125 numerically.

126 3 Beams radiated by uni-variable CSDs

127 The propagation from sources with uni-variable CSD, both in the near and in the far field, can be dealt
128 with starting from their expansion in terms of coherent modes. In such a way, from Eq. (6) we have, at
129 any plane $z = \text{const.}$,

$$W(\mathbf{r}_1, \mathbf{r}_2, z) = \sum_{n=0}^{\infty} \lambda_n \Phi_n(\mathbf{r}_1, z) \Phi_n^*(\mathbf{r}_2, z), \quad (14)$$

130 where the expression of the propagated modes $\Phi_n(\mathbf{r}, z)$ depends on the approximation we use.

131 Using the expression above, the spectral density and the degree of coherence of the radiated field
132 can be evaluated as [55]

$$S(\mathbf{r}, z) \equiv W(\mathbf{r}, \mathbf{r}, z) = \sum_{n=0}^{\infty} \lambda_n |\Phi_n(\mathbf{r}, z)|^2, \quad (15)$$

133 and

$$\mu(\mathbf{r}_1, \mathbf{r}_2, z) \equiv \frac{W(\mathbf{r}_1, \mathbf{r}_2, z)}{\sqrt{S(\mathbf{r}_1, z) S(\mathbf{r}_2, z)}}, \quad (16)$$

134 respectively.

3.1 Coherent modes in paraxial regime

Within the paraxial approximation, the propagation of the modes can be studied through the Fresnel integral, which, for a typical field $V(r, \varphi, z)$, in polar coordinates reads [55]

$$V(r, \varphi, z) = -\frac{ik e^{ikz}}{2\pi z} \int_0^\infty \int_0^{2\pi} V(r', \varphi', 0) e^{i\frac{k}{2z}[r'^2 + r^2 - 2r'r \cos(\varphi' - \varphi)]} r' dr' d\varphi'. \quad (17)$$

Using the equality

$$J_n(t) = \frac{1}{2\pi} \int_0^{2\pi} e^{in\psi - it \sin \psi} d\psi, \quad (18)$$

after some manipulations the propagated modes take the following form:

$$\begin{aligned} \Phi_n(\mathbf{r}, z) = & \frac{2N_F}{r_0} \sqrt{\pi(n+1)} e^{ikz} (-i)^{n+1} \times \\ & e^{in\varphi} e^{i\pi N_F \rho^2} \int_0^1 J_n(2\pi N_F \rho u) e^{i\pi N_F u^2} u^{n+1} du, \end{aligned} \quad (19)$$

where the Fresnel number has been introduced as

$$N_F = \frac{kr_0^2}{2\pi z}, \quad (20)$$

together with the normalized transverse coordinate

$$\boldsymbol{\rho} = \frac{\mathbf{r}}{r_0} = (\xi, \eta). \quad (21)$$

It is seen that the vortex structure of the phase is preserved during propagation and that, once the order n has been set, the propagated field depends only on the Fresnel number, as happens for the diffraction of a plane wave by a circular hole (corresponding to $n = 0$) [61]. Therefore, the Fresnel number will be taken as the natural variable to represent the propagation distance. As examples, density plots of the spectral density of some modes across the plane (x, z) , that is, the squared modulus of the expression in Eq. (19), are shown in Fig. 1.

As a first remark, we note that the property for a CSD of being uni-variable across a certain plane is not preserved during propagation. In fact, when modes propagate, their analytical forms actually change, and, in general, the product of the propagated modes, $\Phi_n(\mathbf{r}_1, z) \Phi_n^*(\mathbf{r}_2, z)$, is no longer proportional to $r_1^n r_2^n \exp[in(\varphi_1 - \varphi_2)]$, as it is required for the series to be interpreted as a power expansion.

Second, as also appears from Fig. 1, the on-axis irradiance is zero for all modes, except $n = 0$. Furthermore, the modes spread during propagation at a rate that increases with n , giving less and less significant contributions in the central zone of the transverse planes. In particular, we expect that, when superpositions of modes are considered, only a finite number of modes need to be taken into account, which depends on the extent of the region where the field has to be evaluated. For example, modes with order 5 or higher can be safely neglected if the field has to be evaluated at $N_F = 0.5$ within a circular region of radius $2r_0$ (see Fig. 1).

3.2 Coherent modes in the far field

Unlike mode propagation in the Fresnel regime, far-field conditions lead to simple analytical forms. When the Fraunhofer conditions are met, the expression of a typical field (say, V_∞) is obtained from the Fourier transform, suitably scaled, of the field across the source [61]. For simplicity, the coordinate across the Fourier plane (say \mathbf{v}) will be taken as the spatial coordinate across a transverse plane in the far zone. Disregarding unessential proportionality factors and curvature terms, we simply write

$$V_\infty(\mathbf{v}) = \iint V(\mathbf{r}, 0) e^{-2\pi i \mathbf{v} \cdot \mathbf{r}} d\mathbf{r}, \quad (22)$$

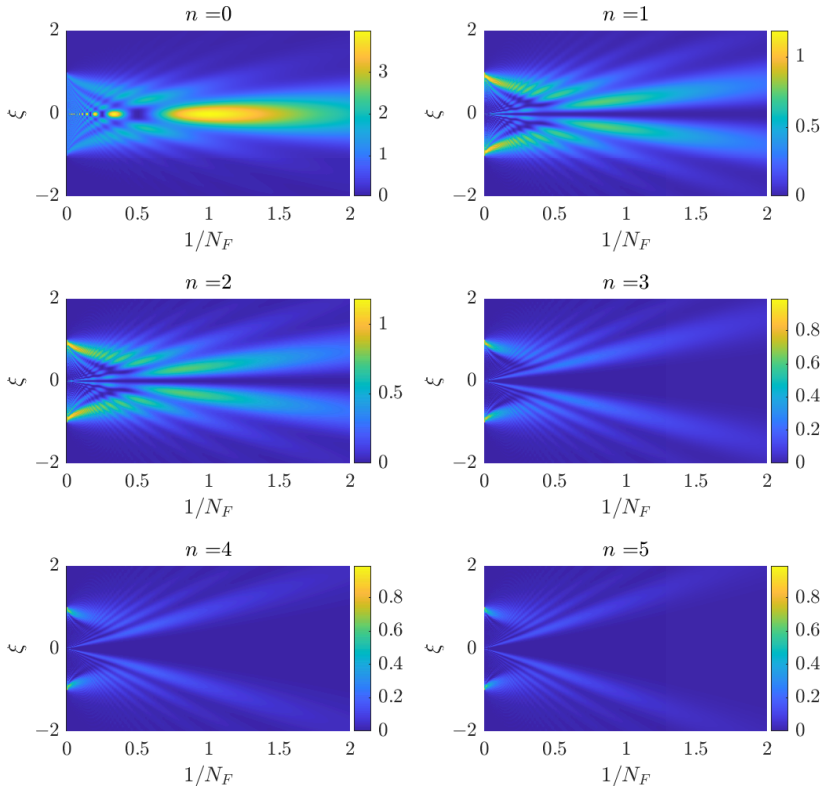


Figure 1. Density plots of the spectral density of some modes, $|\Phi_n(\mathbf{r}, z)|^2$, across the plane (ξ, z) for $n = 0, 1, 2, 3, 4, 5$.

165 the integral extending over the whole $z = 0$ plane.

166 Using polar coordinates, the above integral reads

$$V_\infty(\mathbf{v}) = \int_0^\infty \int_0^{2\pi} V(r, \varphi, 0) e^{-2\pi i \mathbf{v} r \cos(\theta - \varphi)} r dr d\varphi, \quad (23)$$

167 with \mathbf{v} and ϑ the polar coordinates of \mathbf{v} . For the case of the modes in Eq. (7), the above integral gives

$$\Phi_{n,\infty}(\mathbf{v}) = \frac{2(-i)^n}{r_0} \sqrt{\pi(n+1)} e^{in\vartheta} \int_0^{r_0} \left(\frac{r}{r_0}\right)^{n+1} J_n(2\pi \mathbf{v} r) dr, \quad (24)$$

168 J_n being the Bessel function of the first kind and order n [62]. Exploiting the following relation obeyed
169 by the Bessel functions [63]:

$$\frac{d}{d\eta} [\eta^{n+1} J_{n+1}(\eta)] = \eta^{n+1} J_n(\eta), \quad (25)$$

170 the expression of the modes propagated in the far zone takes the simple form

$$\Phi_{n,\infty}(\mathbf{v}) = 2 r_0 (-i)^n \sqrt{\pi(n+1)} e^{in\vartheta} \frac{J_{n+1}(2\pi r_0 \mathbf{v})}{2\pi r_0 \mathbf{v}}. \quad (26)$$

171 Note that for $n = 0$ the latter equation gives rise to the well-known Fraunhofer diffraction pattern from
172 a circular hole [61]. Indeed, for $n = 0$ the vortex field coincides with that of an ordinary plane wave.
173 For $n \neq 0$, we can read Eq. (26) as the diffraction pattern produced by a vortex field that impinges on a
174 circular aperture [48].

175 Plots of the spectral density of the propagated modes of Eq. (26) are given in Fig. 2 for $n =$
176 5, 10, 15. It appears that, in general, the function is very small until its argument reaches values roughly
equal to n , and then slowly goes to zero in an oscillating way.

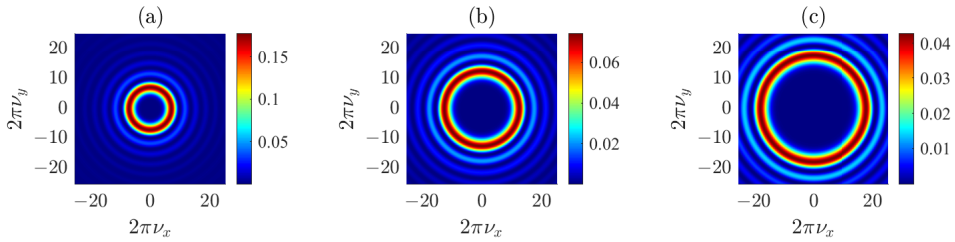


Figure 2. Plots of the spectral density of the modes in the far field, Eq. (26) for $n = 5$ (a), 10 (b), 15 (c), with $r_0 = 1$.

177
178 In light of the above result, it is useful to express the CSD of a beam radiated by a uni-variable
179 source through its Mercer expansion, which reads

$$W_\infty(\nu_1, \nu_2) = 4\pi r_0^2 \sum_{n=0}^{\infty} \lambda_n(n+1) e^{in(\vartheta_1 - \vartheta_2)} \frac{J_{n+1}(2\pi r_0 \nu_1)}{2\pi r_0 \nu_1} \frac{J_{n+1}(2\pi r_0 \nu_2)}{2\pi r_0 \nu_2}. \quad (27)$$

180 In some cases, this expression even leads to closed forms for the degree of coherence in the far field
181 (μ_∞). This happens, for example, if $\lambda_n \propto (n+1)$ and we limit ourselves to point along radial directions
182 (i.e., $\vartheta_1 = \vartheta_2$), in which case it can be shown that [64]

$$\mu_\infty(\nu_1, \vartheta, \nu_2, \vartheta) = 2 \frac{J_1(2\pi r_0(\nu_1 - \nu_2))}{2\pi r_0(\nu_1 - \nu_2)}. \quad (28)$$

183 4 sZegö and truncated sZegö sources

184 The first example of a uni-variable CSD we are going to show is that of the so-called *sZegö source*. The
185 features of such a source across the source plane and in the far zone were studied and commented on
186 in detail in a previous paper [38]. Here we limit ourselves to recall some of the main results obtained
187 there. The effects of paraxial propagation of the radiated field will be studied here on the basis of the
188 expression of the propagated modes obtained in Sec. 3.1. However, we find it convenient to perform
189 such an analysis starting from a different uni-variable CSD, namely, the *truncated sZegö CSD*. Unlike
190 sZegö CSD, in fact, the latter requires a finite number of modes and reduces to sZegö CSD when the
191 number of modes goes to infinity. In such a way, the propagation features of the beams they radiate can
192 be evaluated exactly through finite sums. However, we want to stress that a CSD of this type is interest-
193 ing in itself because it is suitable to be synthesized in the laboratory starting from the superposition of
194 a finite number of coherent fields [20, 28, 32, 37].

195 4.1 The sZegö source

196 To obtain a sZegö CSD we let $c_n = I_0 (\forall n)$ in Eq. (1), with I_0 a positive constant having dimensions of
197 irradiance, so that

$$g(\zeta) = \frac{I_0}{1 - \zeta} \quad (|\zeta| < 1), \quad (29)$$

198 and the corresponding CSD turns out to be

$$W_S(\rho_1, \rho_2, 0) = \frac{I_0}{1 - \rho_1 \rho_2 e^{i(\varphi_1 - \varphi_2)}} \text{circ}(\rho_1) \text{circ}(\rho_2). \quad (30)$$

199 Spectral density and degree of coherence across the source plane turn out to be, from Eqs. (15) and
200 (16),

$$S_S(\rho, 0) = \frac{I_0}{1 - \rho^2} \text{circ}(\rho), \quad (31)$$

201 and

$$\mu_S(\rho_1, \rho_2, 0) = \frac{\sqrt{(1 - \rho_1^2)(1 - \rho_2^2)}}{1 - \rho_1 \rho_2 e^{i(\varphi_1 - \varphi_2)}} \text{circ}(\rho_1) \text{circ}(\rho_2), \quad (32)$$

202 respectively. It can be seen that the spectral density grows to infinite as ρ approaches one. This some-
203 what anomalous behavior has to be ascribed to the fact that an infinite number of modes contribute to
204 the CSD of the source. It will be solved in the next subsection, where the series that gives rise to sZegö
205 source will be truncated. Plots of μ_S (absolute value and phase) are shown in Fig. 3 as a function of ρ_1
206 for fixed ρ_2 . The absolute value of μ_S is seen to vary from 1 (when $\rho_1 = \rho_2$) to 0 (along the circle
207 $\rho_1 = 1$). Furthermore, when ρ_2 is in the center of the source, the phase is constant and equal to 0, while
208 the range of variation of the phase increases with increasing ρ_2 . The presence of a coherence vortex can
209 also be observed, which has charge -1 , centered at a point outside the source at a distance $1/\rho_2$ from
210 the center [38].

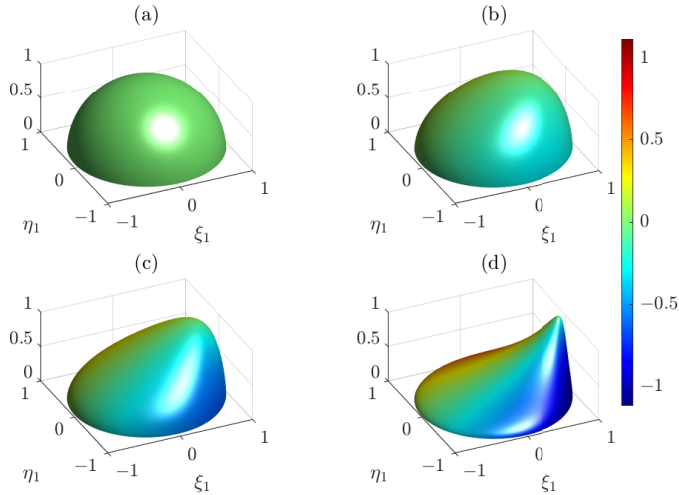


Figure 3. Degree of coherence for a sZegö source at the source plane relative to a point located at (a) $\rho_2 = (0, 0)$; (b) $\rho_2 = (0.3, 0)$; (c) $\rho_2 = (0.6, 0)$; and (d) $\rho_2 = (0.9, 0)$. Absolute value is represented in the vertical axis and the phase is coded in color scale.

211 The OAM degree of coherence at $z = 0$ can be derived using infinite geometric series. Together
212 with the degree of orbitalization they take forms:

$$o_S(\rho_1, \rho_2, 0) = \sqrt{\frac{(1 - \rho_1^2)(1 - \rho_2^2)}{1 - \rho_1^2 \rho_2^2}}; \quad O_S(\rho, 0) = (1 - \rho^2)^2. \quad (33)$$

213 Note that $O_S(\rho, 0)$ has a particularly simple form since for this source $\lambda_n(\rho, 0) \geq \lambda_{n+1}(\rho, 0)$ for all n
214 and ρ , which is not generally true for other source classes. The color density plot of the OAM degree
215 of coherence for this beam is shown in Fig. 4 (a). As expected, this quantity takes the unity value at
216 $\rho_1 = \rho_2 = 0$ but gradually decreases and reaches zero for $\rho_1 = 1$ or $\rho_2 = 1$. We also note that it is not
217 generally unity in the coinciding radii $\rho_1 = \rho_2 \neq 0$, unlike the classic degree of coherence that would be
218 in the coinciding points.

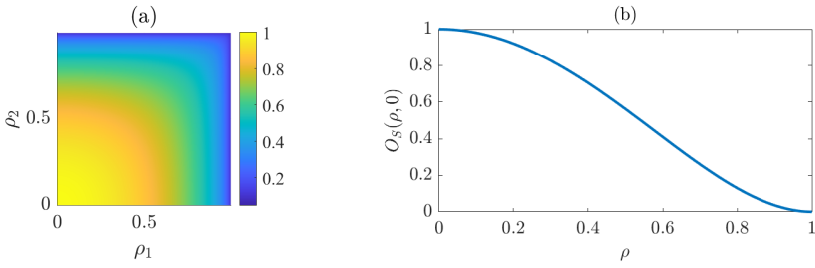


Figure 4. (a) OAM degree of coherence $o_S(\rho_1, \rho_2)$ and (b) degree of orbitalization $O_S(\rho)$ for a sZegö source.

219 An explicit expression of the CSD of the field radiated in the far zone, $W_{S,\infty}$, can hardly be derived
220 directly from the CSD in $z = 0$ but from its modal expansion, with the modes of Eq. (26) and the
221 eigenvalues given by

$$\lambda_n = I_0 \frac{\pi r_0^2}{n+1}, \quad (n = 0, 1, \dots), \quad (34)$$

222 takes the form

$$W_{S,\infty}(\nu_1, \nu_2) \propto \sum_{n=0}^{\infty} \frac{J_{n+1}(2\pi r_0 \nu_1)}{2\pi r_0 \nu_1} \frac{J_{n+1}(2\pi r_0 \nu_2)}{2\pi r_0 \nu_2} e^{in(\theta_1 - \theta_2)}, \quad (35)$$

223 which can be used to evaluate $S_{S,\infty}$ and $\mu_{S,\infty}$ numerically. The latter quantities, evaluated adding the
224 contribution of the first 100 modes, are shown in Figs. 5 and 6, respectively.

225 For the case of the spectral density, it was found that there are no significant differences, at least in
226 the range $r_0 \nu < 1$, when calculating it using only the first 6 modes or the first 100 modes, so that the
227 contribution of modes of order higher than 6 turns out to be negligible. Basically, the same conclusions
228 hold for the degree of coherence, but in such a case the first 10 modes have to be considered. The
229 degree of coherence shows cylindrical symmetry when calculated in relation to the beam axis, with
230 its absolute value reaching a maximum at the center of the beam and showing decreasing oscillations,
231 while the phase alternates between 0 and π . When evaluated in relation to a direction outside the axis,
232 the oscillations of the absolute value of the DOC are distorted and the phase varies gradually. In this
233 case also the presence of coherence vortices can be observed (with charge +1 and -1), corresponding
234 to the zeros of $\mu_{S,\infty}$ [38].

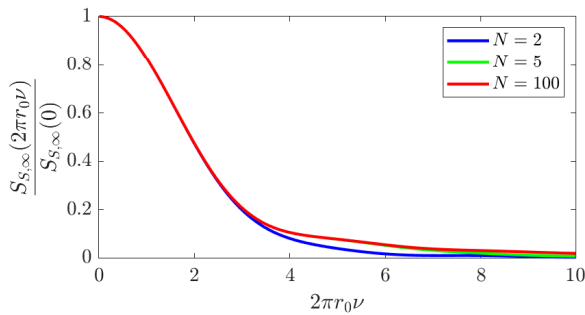


Figure 5. Spectral density for a sZegö source in the far field (with $r_0 = 1$), calculated by adding the first 2, 5 and 100 modes respectively.

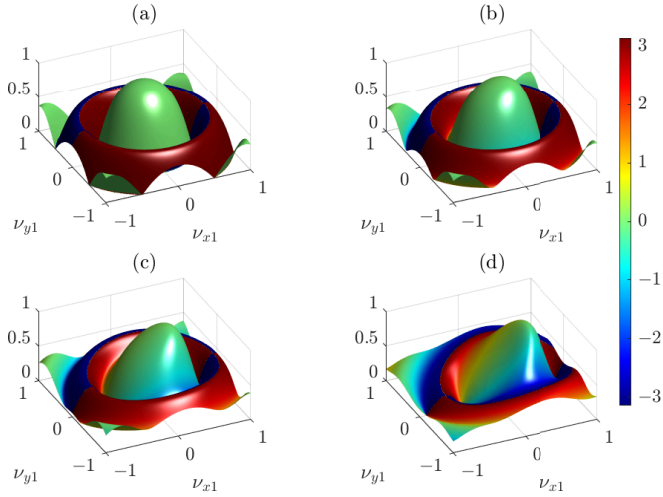


Figure 6. Degree of coherence for a sZegö source across a plane in the far zone relative to a point located at (a) $\nu_2 = (0, 0)$; (b) $\nu_2 = (0.16, 0)$; (c) $\nu_2 = (0.32, 0)$; and (d) $\nu_2 = (0.48, 0)$. Absolute value is represented in the vertical axis and the phase is coded in color scale. The first 100 modes were considered in the calculation.

235 The far-zone OAM degree of coherence of a field radiated by a sZegö source takes form

$$o_S(\nu_1, \nu_2) = \frac{2 \sqrt{\sum_{n=0}^{\infty} J_{n+1}^2(2\pi r_0 \nu_1) J_{n+1}^2(2\pi r_0 \nu_2)}}{\sqrt{1 - J_0^2(2\pi r_0 \nu_1)} \sqrt{1 - J_0^2(2\pi r_0 \nu_2)}}, \quad (36)$$

236 after using a summation formula for $J_{n+1}^2(2\pi r_0 \nu_j)$, $j = 1, 2$ in the denominator. Figure 7(a) shows this
237 quantity as a function of ν_1, ν_2 with $r_0 = 1$, where we restrict ourselves to a region close to the axis.
238 This distribution is structurally different from that in Fig. 4(a), since the coherence no longer decreases
239 monotonically with the increasing radii but oscillates between wider and narrower distributions. It
240 should also be noted that for $\nu_1 = \nu_2 = \nu$ the OAM coherence remains fairly high within the plotted
241 region around the axis.

242 The degree of orbitalization becomes

$$O_S(\nu) = 2 \frac{J_p^2(2\pi r_0 \nu) - J_q^2(2\pi r_0 \nu)}{1 - J_0^2(2\pi r_0 \nu)}, \quad (37)$$

243 where p and q are the indices of the largest and the second largest eigenvalues σ_n for a given radius ν .
244 We note that unlike in the source plane, where the zeroth and the first eigenvalues are the largest and
245 second largest for all radii, in the far field such eigenvalues must be determined numerically. Figure 7(b)
246 shows the degree of orbitalization as a function of ν , with $r_0 = 1$, for $\nu \leq 1$. Unlike in the source plane,
247 where this degree monotonically decreases from unity to zero, see Fig. 4(b), it shows a piece-continuous
248 profile without smoothness at junctions. This is due to the fact that many OAM modes are competing
249 for being the maximum and the second maximum. For example, close to the axis, modes $n = 0$ and
250 $n = 1$ constitute this pair, but at $\nu \approx 0.419$ modes $n = 1$ and $n = 2$ become such. Hence most of the
251 oscillations are due to switching to higher indexes, with one exception: in the region $0.817 \leq \nu \leq 0.894$
252 the $n = 0$ mode has a crest becoming the second largest eigenvalue again.

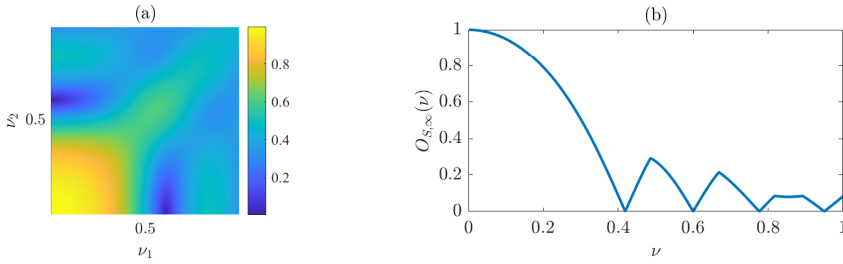


Figure 7. (a) OAM degree of coherence $o_S(v_1, v_2)$; (b) degree of orbitalization $O_S(v)$ for a far field radiated by sZegö source.

4.2 Truncated sZegö sources

In this case, we let $c_n = I_0$ if $0 \leq n < N$ and $c_n = 0$ if $n \geq N$, so that Eq. (1) gives

$$g_T(\zeta) = I_0 \sum_{n=0}^{N-1} \zeta^n = I_0 \frac{1 - \zeta^N}{1 - \zeta} \quad (|\zeta| < 1), \quad (38)$$

and the corresponding CDS turns out to be

$$W_T(\rho_1, \rho_2, 0) = I_0 \frac{1 - (\rho_1 \rho_2)^N e^{iN(\varphi_1 - \varphi_2)}}{1 - \rho_1 \rho_2 e^{i(\varphi_1 - \varphi_2)}}; \quad (0 \leq \rho_1, \rho_2 < 1). \quad (39)$$

Spectral density and degree of coherence across the source plane turn out to be, from Eqs. (15) and (16),

$$S_T(\rho, 0) = I_0 \frac{1 - \rho^{2N}}{1 - \rho^2} \text{circ}(\rho), \quad (40)$$

and

$$\mu_T(\rho_1, \rho_2, 0) = \sqrt{\frac{(1 - \rho_1^2)(1 - \rho_2^2)}{(1 - \rho_1^{2N})(1 - \rho_2^{2N})}} \frac{1 - (\rho_1 \rho_2)^N e^{iN(\varphi_1 - \varphi_2)}}{1 - \rho_1 \rho_2 e^{i(\varphi_1 - \varphi_2)}} \text{circ}(\rho_1) \text{circ}(\rho_2), \quad (41)$$

respectively. The plots of S_T and μ_T are shown in Figs. 8 and 9, respectively. It can be seen that, as the number of modes increases, the spectral density becomes more and more similar to that of the sZegö source but never diverges, as expected. On the other hand, the DOC is highly dependent on the number of modes considered. Two aspects deserve to be noticed.

First, the coherence area decreases as N increases, as expected. The second aspect concerns the phase structure of μ_T . It can be highlighted in a simpler way if we focus our attention onto the second fraction in Eq. (41), being the other terms positive. Using again the variable $\zeta = \rho_1 \rho_2 \exp[i(\varphi_1 - \varphi_2)]$, this term can be written as

$$\frac{1 - \zeta^N}{1 - \zeta} = - \frac{\prod_{n=1}^N (\zeta - \zeta_n)}{1 - \zeta}, \quad (42)$$

where ζ_n ($n = 1, \dots, N$) are the solutions of the equation $\zeta^N = 1$, namely, $\zeta_n = \exp(i2\pi n/N)$. Therefore, since $\zeta_N = 1$, we have

$$- \frac{\prod_{n=1}^N (\zeta - \zeta_n)}{1 - \zeta} = \prod_{n=1}^{N-1} (\zeta - \zeta_n), \quad (43)$$

which for fixed values of ρ_2 and φ_2 can be written as

$$\prod_{n=1}^{N-1} (\zeta - \zeta_n) = \rho_2^{(N-1)} e^{-i(N-1)\varphi_2} \prod_{n=1}^{N-1} \left[\rho_1 e^{i\varphi_1} - \frac{1}{\rho_2} e^{i(\varphi_2 + 2\pi n/N)} \right], \quad (44)$$

270 representing the product of $N-1$ vortices, each having charge $+1$, centered on $N-1$ vertices of a regular
271 enneagon, at a distance $1/\rho_2$ from the center.

272 To better understand this point, let us take $\varphi_2 = 0$. Then, the n -th term of the product takes the form

$$\rho_1 e^{i\varphi_1} - \frac{1}{\rho_2} e^{i2\pi n/N} = \left[\xi_1 - \frac{1}{\rho_2} \cos\left(\frac{2\pi n}{N}\right) \right] + i \left[\eta_1 - \frac{1}{\rho_2} \sin\left(\frac{2\pi n}{N}\right) \right], \quad (45)$$

273 which actually represents a vortex with charge $+1$ and center at

$$\rho_1^{(n)} = \left(\frac{1}{\rho_2} \cos\left(\frac{2\pi n}{N}\right), \frac{1}{\rho_2} \sin\left(\frac{2\pi n}{N}\right) \right). \quad (46)$$

274 The phase structure of the DOC is shown in Fig. 10 for $\rho_2 = (0.9, 0)$ and several values of N .

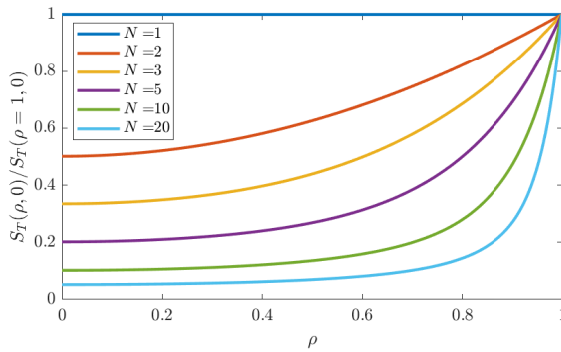


Figure 8. Spectral density at the source (normalized to the maximum) for a truncated sZegö CSD with $N = 1, 2, 3, 5, 10, 20$

275 The OAM degree of coherence for this source at $z = 0$ can be derived using finite geometric series.
276 This quantity and the degree of orbitalization take form

$$o_T(\rho_1, \rho_2, 0) = \sqrt{\frac{(1-\rho_1^2)(1-\rho_2^2)}{1-\rho_1^2\rho_2^2}} \sqrt{\frac{1-\rho_1^{2N}\rho_2^{2N}}{(1-\rho_1^{2N})(1-\rho_2^{2N})}}; \quad O_T(\rho, 0) = \frac{(1-\rho^2)^2}{1-\rho^{2N}}. \quad (47)$$

277 The plots of the OAM degree of coherence for this source are shown in Fig. 11 (a)-(c), for several
278 values of N . Unlike for the sZegö sources the distributions do not decrease to zero for $\rho_1 = 1$ or $\rho_2 = 1$
279 but rather take on values in the interval $(0, 1)$ decreasing with increasing N . The plots of the degree of
280 orbitalization are shown in Fig. 12 for several values of N . The case $N = \infty$ is also shown corresponding
281 to the un-truncated sZegö source. While all the curves have monotonic behavior taking on unit value at
282 $\rho = 0$ and decreasing to zero at $\rho = 1$ only the curve for $N = 1$ is convex on the whole interval, all the
283 others change convexity once.

284 To evaluate the propagated CSD in the near and in the far field Eqs. (14) and (19), or (26) are used.
285 Equations (38) and (8) give, for the eigenvalues,

$$\lambda_n = \begin{cases} I_0 \frac{\pi r_0^2}{n+1} & (0 \leq n < N); \\ 0 & (n \geq N). \end{cases} \quad (48)$$

286 Figure 13 shows examples of the spectral density, across the (x, z) plane, of the field propagated
287 from sZegö sources of various orders. It can be observed that the main contribution for large propagation
288 distances is due to the 0-th order mode (compare Fig. 13 with Fig. 1 for $n = 0$). As commented above,
289 the addition of more and more modes modifies the distribution of the spectral density only for small

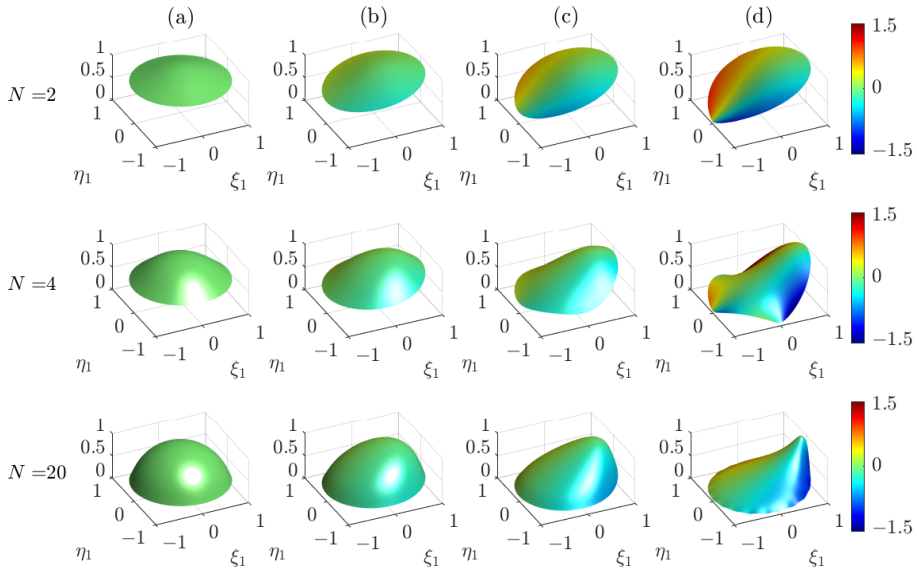


Figure 9. Degree of coherence at the source plane, for a truncated sZegö CSD with $N = 2, 4, 20$ (from top to bottom), relative to a point located at (a) $\rho_2 = (0, 0)$; (b) $\rho_2 = (0.3, 0)$; (c) $\rho_2 = (0.6, 0)$; and (d) $\rho_2 = (0.9, 0)$. Absolute value is represented in the vertical axis and the phase is coded in color scale.

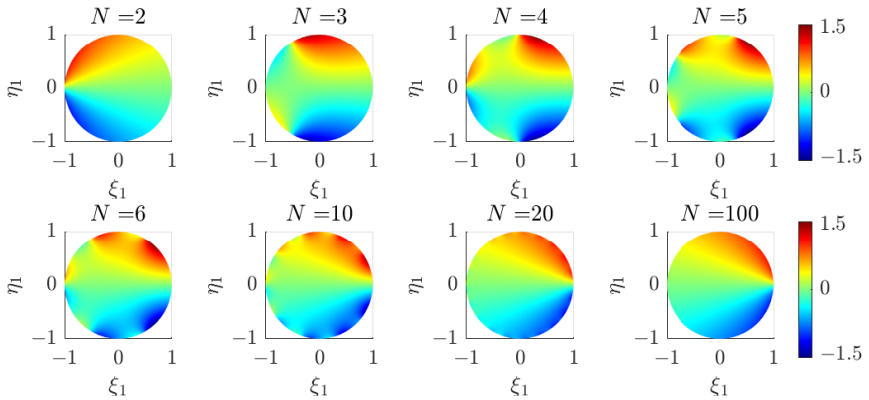


Figure 10. Phase of the degree of coherence at the source plane, for a truncated sZegö CSD relative to the point $\rho_2 = (0.9, 0)$ for several values of N .

290 propagation distances. This is confirmed by the plots in Fig. 14 where the spectral density profiles are
 291 calculated at several propagation distances for sZegö truncated sources with different number of modes.
 292 For a Fresnel number $N_F = 4$, the five profiles are different, although those corresponding to $N = 30$
 293 and $N = 100$ are practically the same up to a normalized distance $\rho = 1$. For $N_F = 1$ the profiles
 294 practically coincide for all truncated sZegö sources with $N \geq 12$. This profile should be the same as the
 295 one for sZegö source.

296 The same approach can be used to evaluate the degree of coherence across different planes (Fig. 15).
 297 The analogous calculations across the source plane and in the far field [38] showed the presence of
 298 coherence vortices (in both cases), and something interesting may happen in between.

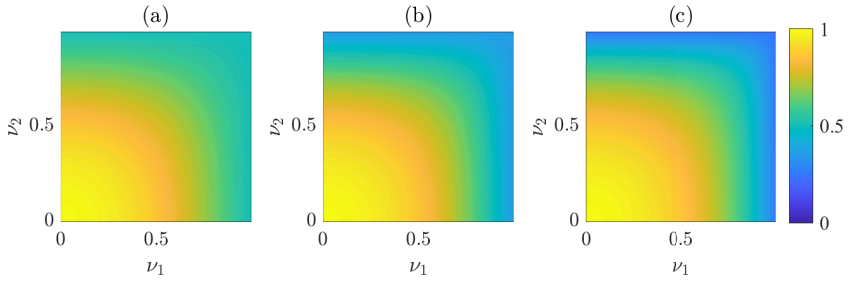


Figure 11. OAM degree of coherence $O_T(\rho_1, \rho_2)$ for truncated sZegö sources with (a) $N = 4$; (b) $N = 8$; (c) $N = 16$.

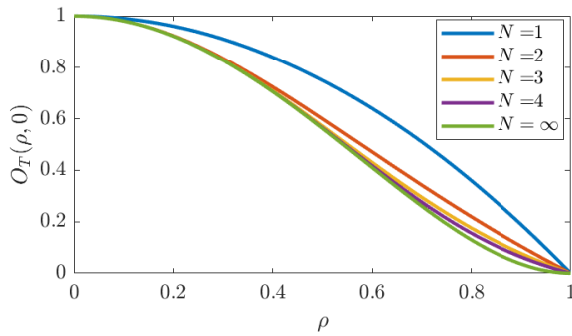


Figure 12. Degree of orbitalization $O_T(\rho)$ for truncated sZegö sources with different values of N . The case $N = \infty$ corresponds to the non-truncated sZegö source.

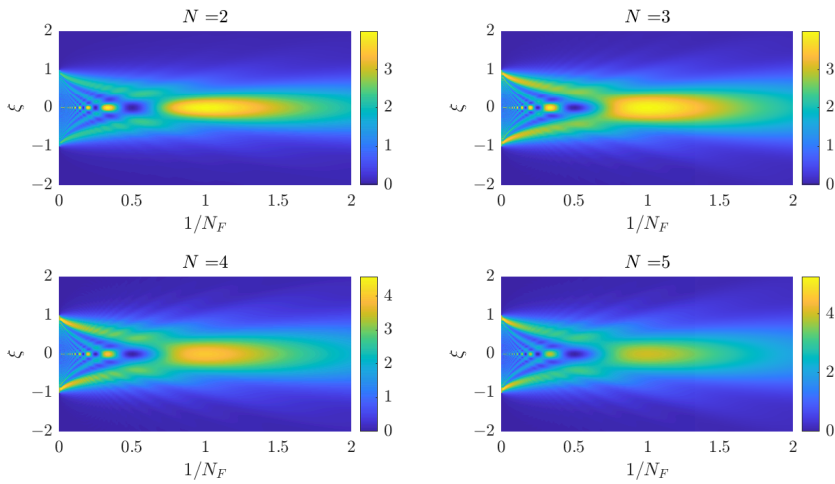


Figure 13. Spectral density versus the inverse of the Fresnel number for several truncated sZegö sources with N modes.

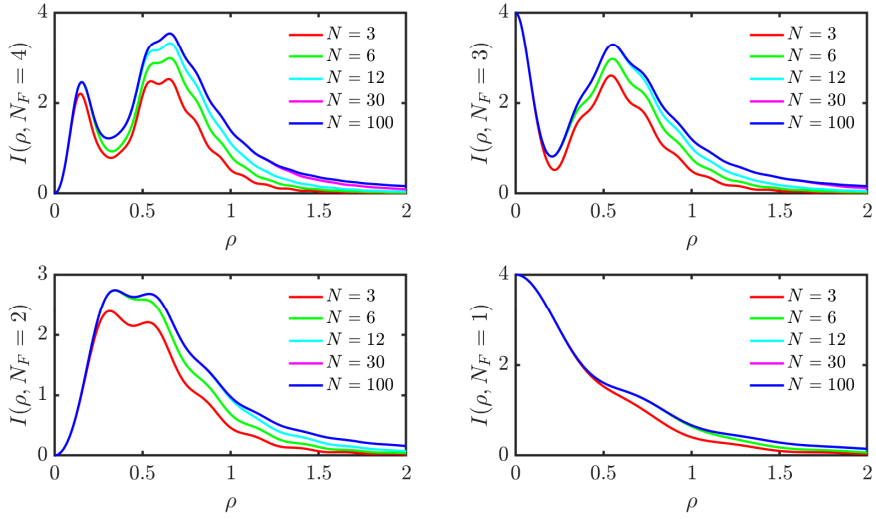


Figure 14. Spectral density versus the inverse of the Fresnel number for different truncated sZegö sources.

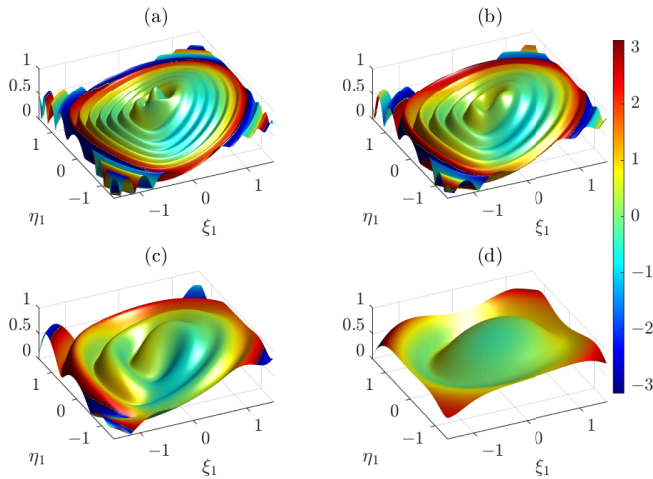


Figure 15. Degree of coherence relative to a point located at $\rho_2 = (0, 0.5)$ for a truncated sZegö source with $N = 4$ at several propagation distances: (a) $N_F = 3$; (b) $N_F = 2$; (c) $N_F = 1$; (d) $N_F = 0.5$. Absolute value is represented in the vertical axis and the phase is coded in color scale.

The far-zone OAM degree of coherence radiated by a truncated sZegö source takes form

$$o_T(v_1, v_2) = \frac{\sqrt{\sum_{n=0}^{N-1} J_{n+1}^2(2\pi r_0 v_1) J_{n+1}^2(2\pi r_0 v_2)}}{\prod_{j=1,2} \sqrt{\sum_{n=0}^{N-1} J_{n+1}^2(2\pi r_0 v_j)}}. \quad (49)$$

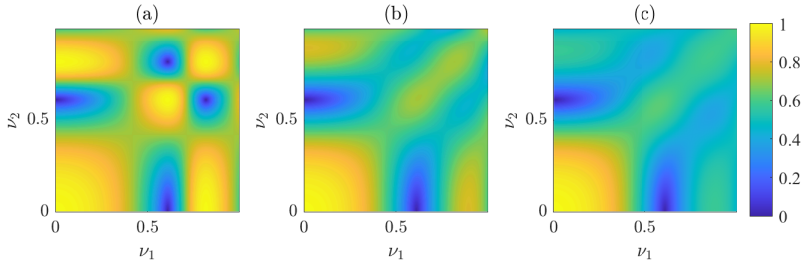


Figure 16. OAM degree of coherence $o_T(v_1, v_2)$ for truncated sZegö far fields with (a) $N = 2$; (b) $N = 3$; (c) $N = 4$.

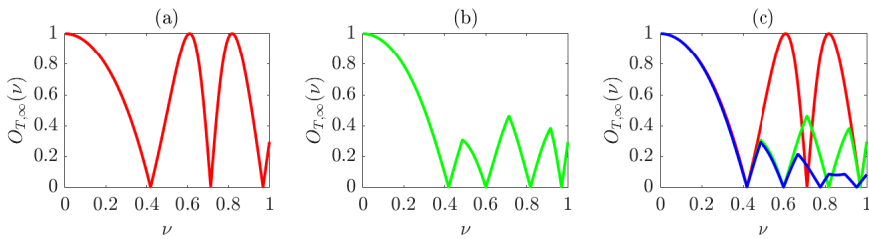


Figure 17. Degree of orbitalization $O_T(\nu)$ for truncated sZegö far fields with: (a) $N = 2$; (b) $N = 3$; (c) combination of $N = 2$, $N = 3$ and non-truncated model.

300 Figure 16 shows this quantity for several values of the summation index: (a) $N = 2$, (b) $N = 3$, and (c)
301 $N = 4$. As N increases, the distributions start resembling that for the non-truncated model, if compared
302 to Fig. 7(a). This practically occurs already for $N = 4$, as higher-order modes deliver much smaller
303 contributions to the sums.

304 For truncated sZegö far fields the degree of orbitalization becomes

$$O_T(\nu) = \frac{J_p^2(2\pi r_0 \nu) - J_q^2(2\pi r_0 \nu)}{\sum_{n=0}^{N-1} J_{n+1}^2(2\pi r_0 \nu)}, \quad (50)$$

305 where, as above, p and q are the indices of the largest and the second largest eigenvalues. Analogously
306 to the non-truncated model, the determination of the largest and the second largest eigenvalues for
307 different radii was carried out numerically.

308 Figure 17 shows formation of the degree of orbitalization for (a) $N = 2$ and (b) $N = 3$. For $N = 2$ the
309 degree exhibits strictly oscillatory nature with smooth maxima and non-smooth minima, all at zeroes.
310 This is due to the fact that only two modes compete with each other for being maximum and second
311 maximum and can only alternate. This behavior is similar to that of the degree of polarization, also
312 involving competition of two electric field components. Starting from $N = 3$ both maxima and minima
313 are not smooth, since the switches are determined by three pairs of modes. Figure 17(c) summarizes
314 the behavior for cases $N = 2$, $N = 3$ and $N \rightarrow \infty$ (non-truncated model), same as in Fig. 7(b).
315 In parts where the curves are almost the same, the same modes act as the largest and second largest
316 eigenvalues resulting in the same numerator in Eq. (17), while the denominator has an increasing value
317 with increasing N . This always occurs at small ν as the 0-th mode always dominates close to the axis.

5 Further examples of uni-variable sources

Different uni-variable CSDs can be defined by choosing different sets of c_n coefficients, and in many cases they are given in closed form, as happened for the case in the previous Section. Actually, using handbooks of mathematical formulas, dozens of other CSDs can be defined from formulas involving power series. Some of them lead to closed forms even when the series is truncated. This is particularly useful because, as we saw for sZegö and truncated sZegö sources, in such a case the effects of truncation can be evaluated quite simply. Furthermore, in any practical realization of partially coherent sources based on the superimposition of perfectly coherent and mutually uncorrelated fields, the number of modes must be necessarily truncated.

Among others, we quote the following (formula 5.2.2.4 of [64]):

$$g(\zeta) = I_0 \sum_{n=1}^{\infty} n \zeta^n = I_0 \frac{\zeta}{(1-\zeta)^2}, \quad (51)$$

together with its truncated version (formula 4.1.7.2 of [64])

$$g_T(\zeta) = I_0 \sum_{n=1}^N n \zeta^n = I_0 \frac{\zeta + (N\zeta - N - 1)\zeta^{N+1}}{(1-\zeta)^2}, \quad (52)$$

with integer N .

Another interesting example of a source obtained with a finite number of modes is that of the *binomial source*, for which (formula 4.2.3.1 of [64])

$$g(\zeta) = I_0 \sum_{n=0}^N \binom{N}{n} \zeta^n = I_0 (1 + \zeta)^N. \quad (53)$$

As a last example, we quote the following, which will be discussed in a little more detail. If we take (formula 5.2.7.2 of [64])

$$g(\zeta) = I_0 \sum_{n=0}^{\infty} \frac{(\gamma^2 \zeta)^n}{n!} = I_0 e^{\gamma^2 \zeta}, \quad (54)$$

with γ^2 a positive dimensionless parameter, the corresponding uni-variable CSD turns out to be

$$W_G(\boldsymbol{\rho}_1, \boldsymbol{\rho}_2) = I_0 \exp\{\gamma^2 \rho_1 \rho_2 \exp[i(\varphi_1 - \varphi_2)]\} \text{circ}(\rho_1) \text{circ}(\rho_2), \quad (55)$$

and the corresponding spectral density has the form

$$S_G(\rho) = I_0 e^{\gamma^2 \rho^2} \text{circ}(\rho). \quad (56)$$

The interest in such sources comes from what follows. If we express W_G through the vectors $\boldsymbol{\rho}_1$ and $\boldsymbol{\rho}_2$, since $\boldsymbol{\rho}_j = (\xi_j, \eta_j)$ and $\rho_j \exp(i\varphi_j) = \xi_j + i\eta_j$, ($j = 1, 2$), Eq. (55) can also be written as

$$\begin{aligned} W_G(\boldsymbol{\rho}_1, \boldsymbol{\rho}_2) &= I_0 e^{\gamma^2(\xi_1 \xi_2 + \eta_1 \eta_2)} e^{-i\gamma^2(\xi_1 \eta_2 - \xi_2 \eta_1)} \text{circ}(\rho_1) \text{circ}(\rho_2) \\ &= I_0 e^{\gamma^2 \rho_1 \rho_2} e^{-i\gamma^2(\boldsymbol{\rho}_1 \times \boldsymbol{\rho}_2)_z} \text{circ}(\rho_1) \text{circ}(\rho_2), \end{aligned} \quad (57)$$

or, after some manipulations,

$$W_G(\boldsymbol{\rho}_1, \boldsymbol{\rho}_2) = I_0 e^{\gamma^2(\rho_1^2 + \rho_2^2)/2} e^{-\gamma^2|\boldsymbol{\rho}_1 - \boldsymbol{\rho}_2|^2/2} e^{-i\gamma^2(\boldsymbol{\rho}_1 \times \boldsymbol{\rho}_2)_z} \text{circ}(\rho_1) \text{circ}(\rho_2), \quad (58)$$

which apparently has the form of a twisted Gaussian Schell-model source with saturated twist [40], the only difference being the sign in the argument of the Gaussian amplitude term. In particular, the degree of coherence turns out to be

$$\mu_G(\boldsymbol{\rho}_1, \boldsymbol{\rho}_2) = e^{-\gamma^2|\boldsymbol{\rho}_1 - \boldsymbol{\rho}_2|^2/2} e^{-i\gamma^2(\boldsymbol{\rho}_1 \times \boldsymbol{\rho}_2)_z} \text{circ}(\rho_1) \text{circ}(\rho_2), \quad (59)$$

342 whose modulus is

$$|\mu_G(\rho_1, \rho_2)| = e^{-\gamma^2 |\rho_1 - \rho_2|^2 / 2} \text{circ}(\rho_1) \text{circ}(\rho_2) . \quad (60)$$

343 The eigenvalues of the Mercer expansion of W_G turn out to be

$$\lambda_n = I_0 \gamma^{2n} \frac{\pi r_0^2}{(n+1)!} , \quad (61)$$

344 from which the propagation features of the radiated beams could be evaluated.

345 In this case, too, the truncated version of the series can be expressed in closed form because (formula 4.1.7.10 of [64])

$$g_T(\zeta) = I_0 \sum_{n=0}^N \frac{(\gamma^2 \zeta)^n}{n!} = I_0 \frac{\Gamma(N+1, \gamma^2 \zeta)}{N!} e^{\gamma^2 \zeta} , \quad (62)$$

347 where $\Gamma(\cdot, \cdot)$ is the incomplete Gamma function [63].

348 6 Conclusions

349 Uni-variable CSDs can be derived from any function of a single complex argument whose Taylor series
 350 involves only non-negative coefficients. The convergence range of the series determines the spatial
 351 extent of the source. The Taylor series can be directly related to the Mercer expansion of the CSD of
 352 the source in such a way that the coherent modes turn out to be optical vortices, restricted to a circle at
 353 the source plane, and the corresponding eigenvalues are proportional to the Taylor coefficients.

354 Although the coherence features of light across the source plane can be directly derived from the
 355 analytical form of the CSD, the analogous properties for the radiated beam can hardly be evaluated
 356 in closed form. Nevertheless, from the knowledge of modes and eigenvalues of the CSD across the
 357 source, the coherence features of the radiated beam can be evaluated both in the Fresnel regime and in
 358 the Fraunhofer regime.

359 In this paper, the tools for studying the properties of the propagated field have been provided and
 360 applied to a test case, that is, the sZegő source. Furthermore, the effects, on the coherence properties
 361 of the source and the radiated field, of truncating the Taylor series have also been investigated. This is
 362 crucial from an experimental point of view, because limiting the Taylor series (i.e., the coherent-mode
 363 expansion of the CSD) to a finite number of terms becomes necessary whenever sources of this kind
 364 have to be synthesized through the superposition of mutually uncorrelated perfectly coherent fields.

365 Since the coherent modes of uni-variable CSDs possess vortex-like structures at various OAM
 366 indices, the overall fields can be regarded as carrying OAM in multiple states. Hence, besides the
 367 spectral density and the degree of coherence, which carry information about correlations in the physical
 368 space, some recently introduced measures, namely, the OAM degree of coherence and the degree of
 369 orbitalization, have also been invoked to characterize solely the radial correlations of the investigated
 370 sources in the OAM space, i.e., the polar Fourier space.

371 Although the technique presented here has been applied to the sZegő CSD and to its truncated
 372 version (the truncated sZegő CSD), it can be applied to any source of the uni-variable type. The number
 373 of uni-variable CSD that can be envisaged starting from the Taylor expansion of a single-argument
 374 function is actually huge, and this work lays the foundation for the design and tailoring of sources with
 375 required coherence characteristics, both on the source plane and in propagation.

376 Funding

377 This work has been supported by Spanish Ministerio de Economía y Competitividad under project
 378 PID2023-148021NB-I00 and Project FASLIGTH (RED2022-134391-T).

379 Conflicts of interest

380 This work has no financial or non-financial competing interests.

381 Data availability statement

382 Data will be made available on request.

383 6.1 Author contribution statement

384 All authors have contributed equally to all aspects of this work, including conceptualization, methodol-
385 ogy, formal analysis, and the writing of the original draft and final manuscript.

386 References

- 387 [1] Yu J, Zhu X, Wang F, Chen Y, Cai Y, Research progress on manipulating spatial co-
388 herence structure of light beam and its applications, *Prog. Quantum Electron.* **91-92**,
389 100486 (2023). <https://doi.org/10.1016/j.pquantelec.2023.100486>
- 390 [2] Rosales-Guzmán C, Rodríguez-Fajardo V, A perspective on structured light's applica-
391 tions, *Appl. Phys. Lett.* **125**, 200503 (2024). <https://doi.org/10.1063/5.0236477>
- 392 [3] Liang C, Wu G, Wang F, Li W, Cai Y, Ponomarenko SA, Overcoming the classical
393 rayleigh diffraction limit by controlling two-point correlations of partially coherent light
394 sources, *Opt. Express* **25**, 28352 (2017). <https://doi.org/10.1364/OE.25.028352>
- 395 [4] Shen Y, Sun H, Peng D, Chen Y, Cai Q, Wu D, Wang F, Cai Y, Ponomarenko SA,
396 Optical image reconstruction in 4f imaging system: Role of spatial coherence structure
397 engineering, *Appl. Phys. Lett.* **118**, 181102 (2021). <https://doi.org/10.1063/5.0046288>
- 398 [5] Gibson G, Courtial J, Padgett MJ, Vasnetsov M, Pas'ko V, Barnett SM, Franke-Arnold
399 S, Free-space information transfer using light beams carrying orbital angular momen-
400 tum, *Opt. Express* **12**, 5448 (2004). <https://doi.org/10.1364/OPEX.12.005448>
- 401 [6] Wang J, Yang JY, Fazal IM, Ahmed N, Yan Y, Huang H, Ren Y, Yue Y, Dolinar S,
402 Tur M et al., Terabit free-space data transmission employing orbital angular momentum
403 multiplexing, *Nat. Photonics* **6**, 488 (2012). <https://doi.org/10.1038/nphoton.2012.138>
- 404 [7] Liu X, Shen Y, Liu L, Wang F, Cai Y, Experimental demonstration of vortex phase-
405 induced reduction in scintillation of a partially coherent beam, *Opt. Lett.* **38**, 5323
406 (2013). <https://doi.org/10.1364/OL.38.005323>
- 407 [8] Gbur G, Partially coherent beam propagation in atmospheric turbulence [invited], *J.*
408 *Opt. Soc. Am. A* **31**, 2038 (2014). <https://doi.org/10.1364/JOSAA.31.002038>
- 409 [9] Lin S, Zhu X, Shen Y, Wang F, Chen X, Gbur G, Cai Y, Yu J, Statistically
410 stationary random light for high-security encryption, *Optica* **12**, 1261 (2025).
411 <https://doi.org/10.1364/OPTICA.546899>
- 412 [10] Zhao C, Cai Y, Trapping two types of particles using a focused partially
413 coherent elegant Laguerre–Gaussian beam, *Opt. Lett.* **36**, 2251 (2011).
414 <https://doi.org/10.1364/OL.36.002251>
- 415 [11] Zhang Z, Liu X, Wang H, Liang C, Cai Y, Zeng J, Flexible optical trapping and manipu-
416 lating rayleigh particles via the cross-phase modulated partially coherent vortex beams,
417 *Opt. Express* **32**, 35051 (2024). <https://doi.org/10.1364/OE.539069>
- 418 [12] Guo J, Ming S, Wu Y, Chen LQ, Zhang W, Super-sensitive rotation measurement with
419 an orbital angular momentum atom-light hybrid interferometer, *Opt. Express* **29**, 208
420 (2021). <https://doi.org/10.1364/OE.409964>
- 421 [13] Gori F, Santarsiero M, Devising genuine spatial correlation functions, *Opt. Lett.* **32**,
422 3531 (2007). <https://doi.org/10.1364/OL.32.003531>
- 423 [14] Martínez-Herrero R, Mejías PM, Gori F, Genuine cross-spectral densities and pseudo-
424 modal expansions, *Opt. Lett.* **34**, 1399 (2009). <https://doi.org/10.1364/OL.34.001399>

- 425 [15] Raghunathan SB, van Dijk T, Peterman EJG, Visser TD, Experimental demonstration
426 of an intensity minimum at the focus of a laser beam created by spatial coherence:
427 application to the optical trapping of dielectric particles, *Opt. Lett.* **35**, 4166 (2010).
428 <https://doi.org/10.1364/OL.35.004166>
- 429 [16] Gbur G, Visser TD, The structure of partially coherent fields, *Prog. Opt.* **55**, 285 (2010).
430 <https://doi.org/10.1016/B978-0-444-53705-8.00005-9>
- 431 [17] Wu G, Cai Y, Detection of a semirough target in turbulent atmosphere by a partially
432 coherent beam, *Opt. Lett.* **36**, 1939 (2011). <https://doi.org/10.1364/OL.36.001939>
- 433 [18] Lajunen H, Saastamoinen T, Propagation characteristics of partially coherent
434 beams with spatially varying correlations, *Opt. Lett.* **36**, 4104 (2011).
435 <https://doi.org/10.1364/OL.36.004104>
- 436 [19] Cai Y, Chen Y, Wang F, Generation and propagation of partially coherent beams with
437 nonconventional correlation functions: a review [invited], *J. Opt. Soc. Am. A* **31**, 2083
438 (2014). <https://doi.org/10.1364/JOSAA.31.002083>
- 439 [20] Rodenburg B, Mirhosseini M, Magaña-Loaiza OS, Boyd RW, Experimental generation
440 of an optical field with arbitrary spatial coherence properties, *J. Opt. Soc. Am. B* **31**,
441 A51 (2014). <https://doi.org/10.1364/JOSAB.31.000A51>
- 442 [21] Divitt S, Novotny L, Spatial coherence of sunlight and its implications for light manage-
443 ment in photovoltaics, *Optica* **2**, 95 (2015). <https://doi.org/10.1364/OPTICA.2.000095>
- 444 [22] Chen Y, Ponomarenko SA, Cai Y, Experimental generation of optical coherence lattices,
445 *Appl. Phys. Lett.* **109**, 061107 (2016). <https://doi.org/10.1063/1.4960966>
- 446 [23] M.W. Hyde IV MW, Bose-Pillai SR, Wood RA, Synthesis of non-uniformly correlated
447 partially coherent sources using a deformable mirror, *Appl. Phys. Lett.* **111**, 101106
448 (2017). <https://doi.org/10.1063/1.4994669>
- 449 [24] Santarsiero M, Martínez-Herrero R, Maluenda D, de Sande JCG, Piquero G, Gori F,
450 Partially coherent sources with circular coherence, *Opt. Lett.* **42**, 1512 (2017).
451 <https://doi.org/10.1364/OL.42.001512>
- 452 [25] Santarsiero M, Martínez-Herrero R, Maluenda D, de Sande JCG, Piquero G,
453 Gori F, Synthesis of circularly coherent sources, *Opt. Lett.* **42**, 4115 (2017).
454 <https://doi.org/10.1364/OL.42.004115>
- 455 [26] Ding C, Koivurova M, Turunen J, Pan L, Self-focusing of a partially coherent
456 beam with circular coherence, *J. Opt. Soc. Am. A* **34**, 1441 (2017).
457 <https://doi.org/10.1364/JOSAA.34.001441>
- 458 [27] Piquero G, Santarsiero M, Martínez-Herrero R, de Sande JCG, Alonzo M, Gori F,
459 Partially coherent sources with radial coherence, *Opt. Lett.* **43**, 2376 (2018).
460 <https://doi.org/10.1364/OL.43.002376>
- 461 [28] Chen X, Li J, Rafsanjani SMH, Korotkova O, Synthesis of I_m -Bessel correlated beams
462 via coherent modes, *Opt. Lett.* **43**, 3590 (2018). <https://doi.org/10.1364/OL.43.003590>
- 463 [29] Wu D, Wang F, Cai Y, High-order nonuniformly correlated beams, *Opt. Laser Technol.*
464 **99**, 230 (2018). <https://doi.org/10.1016/j.optlastec.2017.09.007>
- 465 [30] Martínez-Herrero R, Piquero G, de Sande JCG, Santarsiero M, Gori F, Besinc
466 pseudo-Schell model sources with circular coherence, *Appl. Sci.-Basel* **9** (2019).
467 <https://doi.org/10.3390/app9132716>
- 468 [31] de Sande JCG, Martínez-Herrero R, Piquero G, Santarsiero M, Gori F, Pseudo-Schell
469 model sources, *Opt. Express* **27**, 3963 (2019). <https://doi.org/10.1364/OE.27.003963>
- 470 [32] Zhu X, Yu J, Chen Y, Wang F, Korotkova O, Cai Y, Experimental synthesis of random
471 light sources with circular coherence by digital micro-mirror device, *Appl. Phys. Lett.*
472 **117**, 121102 (2020). <https://doi.org/10.1063/5.0024283>

- 473 [33] Martínez-Herrero R, Santarsiero M, Piquero G, de Sande JCG, A new type of shape-
474 invariant beams with structured coherence: Laguerre-Christoffel-Darboux beams, *Photonics* **8** (2021). <https://doi.org/10.3390/photonics8040134>
475
- 476 [34] Santarsiero M, Martínez-Herrero R, Piquero G, de Sande JCG, Gori F,
477 Modal analysis of pseudo-Schell model sources, *Photonics* **8** (2021).
478 <https://doi.org/10.3390/photonics8100449>
- 479 [35] Martínez-Herrero R, Piquero G, Santarsiero M, Gori F, de Sande JCG, A class of vecto-
480 rial pseudo-Schell model sources with structured coherence and polarization, *Opt. Laser*
481 *Technol.* **152**, 108079 (2022). <https://doi.org/10.1016/j.optlastec.2022.108079>
- 482 [36] Korotkova O, Gbur G, in *A Tribute to Emil Wolf*, edited by T.D. Visser (Elsevier, 2020),
483 Vol. 65 of *Prog. Opt.*, pp. 43–104.
- 484 [37] Moreno-Acosta P, Rickenstorff-Parrao C, Ramirez-San-Juan JC, Rosales-Guzman C,
485 Ramos-Garcia R, Experimental generation of partially coherent besinc pseudo-Schell
486 model sources using a digital micromirror device, *J. Opt. Soc. Am. B* **42**, 1804 (2025).
487 <https://doi.org/10.1364/JOSAB.564315>
- 488 [38] Gori F, Santarsiero M, Martínez-Herrero R, Uni-variable cross-spectral densities, *Opt.*
489 *Laser Technol.* **180**, 111511 (2025). <https://doi.org/10.1016/j.optlastec.2024.111511>
- 490 [39] Indebetouw G, Optical vortices and their propagation, *J. Mod. Opt.* **40**, 73 (1993).
491 <https://doi.org/10.1080/09500349314550101>
- 492 [40] Simon R, Mukunda N, Twisted Gaussian Schell-model beams, *J. Opt. Soc. Am. A* **10**,
493 95 (1993). <https://doi.org/10.1364/JOSAA.10.000095>
- 494 [41] Gori F, Santarsiero M, Borghi R, Vicalvi S, Partially coherent sources with helicoidal
495 modes, *J. Mod. Opt.* **45**, 539 (1998). <http://dx.doi.org/10.1080/09500349808231913>
- 496 [42] Ponomarenko SA, A class of partially coherent beams carrying optical vortices, *J. Opt.*
497 *Soc. Am. A* **18**, 150 (2001). <https://doi.org/10.1364/JOSAA.18.000150>
- 498 [43] Gbur G, Visser TD, Coherence vortices in partially coherent beams, *Opt. Commun.* **222**,
499 117 (2003). [https://doi.org/10.1016/S0030-4018\(03\)01606-7](https://doi.org/10.1016/S0030-4018(03)01606-7)
- 500 [44] Tamburini F, Anzolin G, Umbriaco G, Bianchini A, Barbieri C, Overcoming the
501 Rayleigh criterion limit with optical vortices, *Phys. Rev. Lett.* **97**, 163903 (2006).
502 <https://doi.org/10.1103/PhysRevLett.97.163903>
- 503 [45] Franke-Arnold S, Allen L, Padgett M, Advances in optical angular momentum, *Laser*
504 *& Photonics Rev.* **2**, 299 (2008). <https://doi.org/10.1002/lpor.200810007>
- 505 [46] Padgett M, Bowman R, Tweezers with a twist, *Nat. Photonics* **5**, 343 (2011).
506 <https://doi.org/10.1038/nphoton.2011.81>
- 507 [47] Mirhosseini M, Magaña-Loaiza OS, Chen C, Rodenburg B, Malik M, Boyd RW, Rapid
508 generation of light beams carrying orbital angular momentum, *Opt. Express* **21**, 30196
509 (2013). <https://doi.org/10.1364/OE.21.030196>
- 510 [48] Ambuj A, Vyas R, Singh S, Diffraction of orbital angular momentum carry-
511 ing optical beams by a circular aperture, *Opt. Lett.* **39**, 5475 (2014).
512 <https://doi.org/10.1364/OL.39.005475>
- 513 [49] Gbur G, *Singular Optics*, 1st edn. (CRC Press, 2016), ISBN 978-0521642224
- 514 [50] Zeng J, Lin R, Liu X, Zhao C, Cai Y, Review on partially coherent vortex beams, *Front.*
515 *Optoelectron.* **12**, 229 (2019). <https://doi.org/10.1007/s12200-019-0901-x>
- 516 [51] Zhang Y, Cai Y, Gbur G, Control of orbital angular momentum with partially coherent
517 vortex beams, *Opt. Lett.* **44**, 3617 (2019). <https://doi.org/10.1364/OL.44.003617>
- 518 [52] Liu X, Zeng J, Cai Y, Review on vortex beams with low spatial coherence, *Adv. Phys.:*
519 *X* **4**, 1626766 (2019). <https://doi.org/10.1080/23746149.2019.1626766>

- 520 [53] Zhang H, Lu X, Wang Z, Konijnenberg AP, Wang H, Zhao C, Cai Y, Generation and
521 propagation of partially coherent power-exponent-phase vortex beam, *Front. Phys.* **9** -
522 **2021** (2021). <https://doi.org/10.3389/fphy.2021.781688>
- 523 [54] Hyde IV MW, Korotkova O, Spencer MF, Partially coherent sources whose co-
524 herent modes are spatiotemporal optical vortex beams, *J. Opt.* **25**, 035606 (2023).
525 <https://doi.org/10.1088/2040-8986/acba2d>
- 526 [55] Mandel L, Wolf E, *Optical Coherence and Quantum Optics* (Cambridge University
527 Press, 1995), ISBN 9780521417112
- 528 [56] Siegman AE, *Lasers* (University Science Books, 1986), ISBN 0935702113
- 529 [57] Korotkova O, Gbur G, Unified matrix representation for spin and orbital angu-
530 lar momentum in partially coherent beams, *Phys. Rev. A* **103**, 023529 (2021).
531 <https://doi.org/10.1103/PhysRevA.103.023529>
- 532 [58] Korotkova O, Pokharel S, OAM degree of coherence, *Opt. Lett.* **49**, 5103 (2024).
533 <https://doi.org/10.1364/OL.528291>
- 534 [59] Korotkova O, Orbitalization ellipse of a light beam, *Opt. Lett.* **50**, 391 (2025).
535 <https://doi.org/10.1364/OL.545613>
- 536 [60] Korotkova O, Orbitalization structure of random light beams, *J. Opt.* **27**, 065606 (2025).
537 <https://doi.org/10.1088/2040-8986/addc7c>
- 538 [61] Born M, Wolf E, *Principles of Optics*, seventh (corrected) edn. (Cambridge University
539 Press, 1999), ISBN 978-0521642224
- 540 [62] Gradshteiin IS, Ryzhik IM, *Table of Integrals, Series, And Products*, 4th edn. (Academic
541 Press, 1965)
- 542 [63] Abramowitz M, Stegun I, eds., *Handbook of mathematical functions* (Dover Publica-
543 tions Inc, 1972)
- 544 [64] Prudnikov A, Brychkov Y, Marichev O, *Integrals and Series, Vol.1: Elementary Func-*
545 *tions* (Gordon and Breach Science Publisher, 1986)